Nanoscale Advances

PAPER

View Article Online
View Journal | View Issue

Cite this: *Nanoscale Adv.*, 2019, **1**, 2382

CdS nanodroplets over silica microballs for efficient room-temperature LPG detection†

Nupur Saxena, *[a] Pragati Kumar *[b] and Vinay Gupta [c]

An efficient room-temperature sensor for liquified petroleum gas (LPG) is demonstrated by employing CdS:SiO_2 nanocomposite thin films (CdS:SiO_2 NCTFs) for the first time. CdS:SiO_2 NCTFs exhibiting the morphology of CdS nanodroplets on micron-sized spherical balls of SiO_2 were deposited using the pulsed laser deposition (PLD) method, followed by thermal annealing. The targets of chemically synthesized CdS nanoparticles and commercially procured SiO_2 were used to deposit CdS:SiO_2 NCTFs by swapping them at a frequency ratio of 2 : 8 laser pulses per second, which was selected to ensure nearly the same ratio of CdS to SiO_2 in NCTFs and was confirmed by X-ray photoelectron spectroscopy. Sensor fabrication was carried out on bare CdS thin films and as-grown and annealed CdS:SiO_2 NCTFs using an Ag paste over Pt interdigitated electrodes to measure the resistance of the films in air and in the presence of reducing gases, *viz.*, LPG, H_2, H_2S, NO_2 and CO_2. The present sensor showed the highest response for LPG and the observed value was ~71% for 1000 ppm at RT with the response time and recovery time of 91 s and 140 s, respectively. The response of the sensor was sustainable up to 75 °C and then decreased, which suggested its promising usage for low-temperature regions as well. A low detection limit of 20 ppm at RT for LPG was determined; however, a significant response was observed only at 50 ppm. The sensor retained ~96% of its initial response even after 8 weeks and that too at 100 °C. The present LPG sensor is highly promising due to its high sensitivity, low detection limit, low response and recovery times, good reproducibility, RT operation and simple fabrication technique.

Received 28th January 2019
Accepted 24th April 2019

DOI: 10.1039/c9na00053d

rsc.li/nanoscale-advances

1. Introduction

Liquefied petroleum gas (LPG) is one of the highly flammable gases and its usage as a fuel gas in homes, workplaces, and industries including those of automobiles is increasing day by day all over the world. Evidently, the casualties are also increasing and are manifold due to its leakage/bursting. According to a report by the National Fire Protection Association (NFPA), USA, in 2007–2011, U.S. municipal fire departments responded to an estimated average of 51 600 fires per year involving the ignition of a flammable gas as the type of material first ignited; these cases included 20 260 fires per year in homes and 31 340 fires per year at other properties. These fires cause an estimated 168 civilian deaths per year, 1029 civilian injuries per year, and losses of $644 million per year in direct property damage.[1]

As far as India is concerned, the total number of accidental deaths by cooking gas cylinder/stove explosions was 3525 in 2014, which increased to 3667 in 2015 according to the National Crime Records Bureau. More than 3 lakh deaths were reported due to fire-related incidents, with an average of 59 deaths per day between 2000 and 2016 in India.[2] Fig. 1 shows the fact sheets of fires caused by flammable gases in the USA, which indicates that an average of 28% fire accidents in home and non-home structures is due to the leakage of LPG only, whereas 17% fire accidents are due to the bursting of cylinder/stoves in India. The pie chart in Fig. 1b shows the causes responsible for fires in India in percentage. The percentages of civilian deaths, injuries and property damages are depicted in Fig. 1a as a bar diagram. The statistics of deaths caused by fire from 2000 to 2016 in the USA, UK and India are shown in Fig. 1b. Indeed, the number of deaths in India is quite high with respect to that in developed countries such as the USA and UK; however, these data are comparable with respect to the population of the respective countries. For illustration, the fire death rate in India is twice that in the USA. However, the fire death rate in Russia is 3.5 times that in India; also, in European countries like Belarus and Lithuania, it is 4 times and 2.5 times, respectively, than that in India.[3] Therefore, fire safety is a critical issue not just in developing countries such as India but all over the world.

[a]*Department of Physics & Astronomical Sciences, Central University of Jammu, Rahya-Suchani (Bagla), Samba, 181 143 Jammu, J&K, India. E-mail: n1saxena@gmail.com; Tel: +91-9797872397*

[b]*Department of Nano Sciences and Materials, Central University of Jammu, Rahya-Suchani (Bagla), Samba, 181 143 Jammu, J&K, India. E-mail: pkumar.phy@gmail.com; Tel: +91-9055180885*

[c]*Department of Physics & Astrophysics, University of Delhi, Delhi-110 007, India*

† Electronic supplementary information (ESI) available. See DOI: 10.1039/c9na00053d

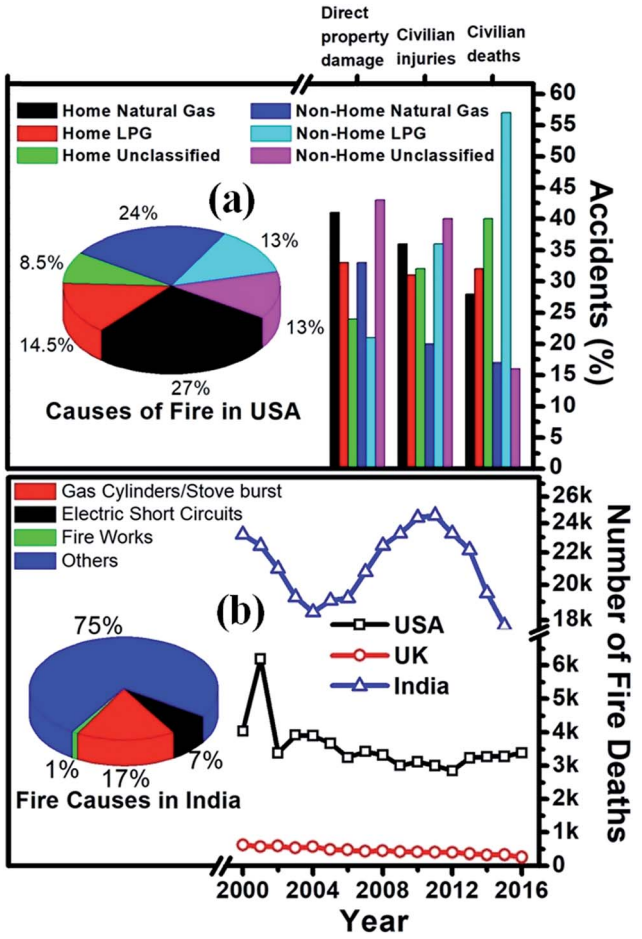

Fig. 1 (a) Fact sheet of fires caused with flammable gases in the USA and (b) year-wise fire deaths in USA, UK and India. Pie charts of fire causes in (a) USA and (b) India.

To monitor, detect and precisely measure trace levels of LPG in the environment and for early warning systems, the development of a reliable sensor with improved sensitivity and selectivity is crucial for preventing fatal accidents. Another crucial parameter, particularly for a flammable gas sensor, is its operating temperature. The operating temperature of such a sensor should be preferably low as a high operating temperature will require a complex sensing platform and may lead to explosion due to the presence of explosive gases in the confined area. In contrast, a low operating temperature will help the superficial fabrication of portable gadgets with the least chance of detonation.

It has been proven that nanoscale materials have the potential for chemical, gas and biological sensing due to their highly tunable size- and shape-dependent chemical and physical properties.[4] Principally, their large surface areas and high pore volumes per unit mass increase the sensitivity and the response times of sensors. Enormous efforts have been made to develop a gas sensor with high sensitivity, high selectivity, short response and recovery times and most importantly a low operating temperature using diverse materials to detect noxious, explosive, inflammable and pollutant gases.[5–10] However, the invention of semiconductor-based sensing devices with identical desired parameters to identify hazardous gases for a healthy ambience is still an open challenge for researchers. Many successful efforts have been made to achieve a low operating temperature using a variety of nanomaterials; their hybrid structures and composite materials have even been demonstrated to work at room temperature (RT).[6–11] This particular feature is typically observed in CdS nanocomposites or CdS heterostructures. Nevertheless, the other sensing parameters, *viz.*, the response and recovery times, sensitivity, and detection limit depend on other composite or heterostructure materials. Dhawale *et al.*[6] fabricated an LPG sensor based on an *n*-CdS/p-polyaniline thin film heterojunction using a simple inexpensive electrodeposition technique. Their sensor could detect LPG at RT with a gas response of 80% and it exhibited 95% stability on exposure to 1040 ppm concentration of gas. A comparative assessment of the performances of CdS/polyacrylamide and $Cd(NO_3)_2 \cdot (AAm)_4 \cdot 2H_2O$ thick films for LPG sensing at RT was investigated by Singh *et al.*[7] They observed maximum sensitivities of 1.3 and 3.7 GΩ min^{-1} for CdS/polyacrylamide and $Cd(NO_3)_2 \cdot (AAm)_4 \cdot 2H_2O$, respectively. The response and recovery times were recorded as 2 and 8 min, respectively, for 5 vol% (50 000 ppm) of LPG. Surface-coated PbS nanoparticles on CdS nanowires with a high-surface-area nano-heterojunction were synthesized chemically and exposed to LPG at RT by Sonawane *et al.*[8] The architecture exhibited a gas response of 60% on exposure to 1200 ppm of LPG; the response and recovery times were 120 s and 105 s, respectively, and a stable response of 93% for up to 10 days was observed. In another study on a chemically synthesized PEDOT:PSS shell on CdS nanowires reported by Sonawane *et al.*,[9] they observed almost the same gas response (58.9%) and response and recovery times of 126 s and 109 s, respectively, under exposure to a relatively low gas concentration (900 ppm). Lokhande *et al.*[10] examined the performance of a Cu_2SnS_3 (CTS)/CdS heterojunction for LPG sensing and observed a maximum LPG response of 56% at RT after exposure to 780 ppm gas with 31 s and 56 s response and recovery times, respectively. This device retained 95% gas sensing stability after a time period of 60 days. The existing literature indicates that the manipulation with diverse materials/compositions can improve a few parameters with the compensation of other desired parameters. Therefore, the fabrication of sensors using a variety of materials to achieve superior properties is a subject of constant research interest. To the best of our knowledge, bare CdS thin films and CdS:SiO_2 nanocomposite thin films (CdS:SiO_2 NCTFs) have never been tested using such gases.

In this article, we explored pulsed laser-deposited nanocrystalline CdS thin films (nc-CdS) and CdS:SiO_2 NCTFs for LPG sensing. The gas sensing properties of the films were explored for a variety of gases, *viz.*, LPG, H_2, H_2S, NO_2, and CO_2 at RT = 20 °C. All the films showed significant responses for LPG; indeed, the response of CdS:SiO_2 NCTF annealed at 400 °C was much higher than those of others with significantly smaller response and recovery times due to the presence of CdS nanodroplets (NDs) on silica microballs (MBs).

2. Experimental section

2.1 Thin film deposition

The procedure used here for the growth of nc-CdS and CdS:SiO_2 NCTFs by pulsed laser deposition (PLD) setup is fully described elsewhere.[12,13] All the samples investigated were synthesized by PLD by guiding and focusing the third harmonic of a continuum Nd:YAG laser of energy 220 mJ at a wavelength of 355 nm with a repetition rate of 10 Hz and a pulse width of 10 ns onto the rotating target mounted at an oblique angle of 30° to the direction of the incident laser beam. For CdS thin film deposition, chemically synthesized CdS quantum dot (QD)[14] pellets were used as a target, whereas a commercially purchased (Sigma Aldrich Ltd., USA) SiO_2 target was also used along with a CdS target to deposit CdS:SiO_2 NCTFs. N-type ⟨100⟩ Si wafers and carbon-coated Cu TEM grids were used as substrates for deposition and stored at room temperature inside a clean stainless steel vacuum chamber at a base pressure of 5×10^{-6} mbar. CdS:SiO_2 NCTFs of thickness ~500 nm were deposited by exposing the CdS and SiO_2 targets alternatively for 2 and 8 shots of the laser, respectively. The distance between the target and the substrate was 4 cm. The deposition rate of CdS:SiO_2 NCTFs in this configuration was about ~0.20 nm per pulse. Furthermore, thermal annealing of the films was carried out at temperatures of 400 °C and 500 °C for 3 h in an Ar environment to evolve the structural phase of CdS. The sensors fabricated using nc-CdS, CdS:SiO_2 NCTFs pristine annealed at 400 °C and 500 °C temperatures are referred as S_0, S_1, S_2 and S_3, respectively, hereafter

2.2 Characterizations

Structural and optical studies were carried out using basic characterization techniques, *viz.*, glancing angle X-ray diffraction with Cu K_α of wavelength 1.54 Å, micro-Raman spectroscopy, transmission electron microscopy (TEM), X-ray photoelectron spectroscopy (XPS) and photoluminescence (PL) spectroscopy and are reported elsewhere in detail.[12,13] The temperature-dependent photoluminescence study in the temperature range of 20–560 K was carried out to explore the temperature sensing properties of the nanocomposite films.[15]

In the present study, the surface morphology and microstructure of the films were analyzed using scanning electron microscopy (SEM), MIRA\\TESCAN FESEM.

2.3 Gas-sensing measurements

The Pt interdigitated electrodes (IDEs) are patterned over the CdS or CdS:SiO_2 films using conventional photolithography to form a metal–semiconductor–metal (MSM) structure. The gas sensing measurements were carried out. The LPG gas sensing characteristics of the fabricated sensors were studied at RT = 20 °C and relative humidity of ≈60% in a specially designed "Gas Sensor Measurement and Calibration system (GSMCS)" having a glass test chamber of 11 liter volume. Different concentrations of the LPG gas (1 to 1000 ppm) were introduced into the glass test chamber using calibrated leaks through needle valves. A pressure of $\approx 10^{-3}$ torr was first created in the test chamber using a rotary pump and was measured by a Pirani gauge; subsequently, a mixture of the known concentrations of the target gas and clean (dry synthetic) air were introduced till the test chamber acquired atmospheric pressure. At the time of recovery of the sensor, the target gas was flushed out of the test chamber and clean dry air was introduced.

The gas-sensing characteristics were recorded with reference to time at different operating temperatures and gas concentrations. The change in the electrical resistance was recorded after every second using a data acquisition system consisting of a digital multi-meter (model: Keithley 2400) interfaced with a computer and used as a measure of the gas response at various temperatures. The sensor response (% S) for a gas is defined as follows:[5,7,11]

$$\%S = \frac{|R_a - R_g|}{R_a} \times 100 \quad (1)$$

Here, R_a and R_g are the sensor resistances in the presence of atmospheric air and target gas, respectively.

3. Results and discussion

3.1 Surface morphological studies

The surface micrographs of nc-CdS and CdS:SiO_2 NCTFs are depicted in Fig. 2(a) and (b–d), respectively. It is evident from Fig. 2(a) that the surface of the nc-CdS thin film is very smooth with negligible porosity and it is difficult to estimate the particle size. However, the average particle size (APS) values estimated by other techniques such as AFM and TEM are ~9.4 nm and 9.16 nm, respectively, and reported elsewhere[12] (please see ESI Fig. S1†). The morphology of the pristine CdS:SiO_2 nanocomposite film shows micron-sized balls of SiO_2 covered with gel-like CdS or web-like structures (Fig. 2(b)). The growth of CdS

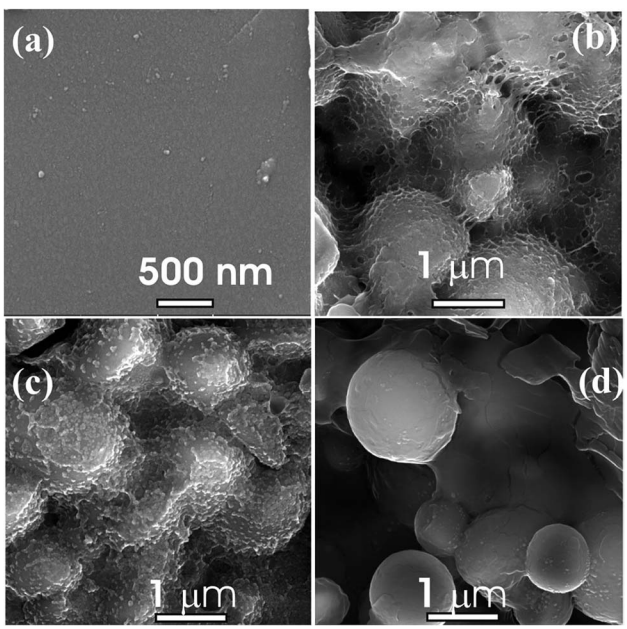

Fig. 2 FESEM micrographs of (a) nc-CdS and (b–d) pristine, annealed at 400 °C and anealed at 500 °C CdS:SiO_2 NCTFs respectively.

NDs can be seen over silica MBs inside the web-like structure in the case of CdS:SiO_2 NCTFs annealed at 400 °C (Fig. 2(c)). It is evident from Fig. 2(c) that SiO_2 MBs are covered/decorated with highly dense CdS NDs with good porosity. Furthermore, the rise in the annealing temperature from 400 °C to 500 °C results in reduction in the density of CdS NDs on the surface of SiO_2 MBs along with reduction in the porosity and evaporation of the web-like structures.

The energy-dispersive X-ray (EDX) spectra of CdS:SiO_2 NCTFs annealed at 400 °C and 500 °C taken at different regions are shown in Fig. 3(a–d). As illustrated in Fig. 3(a–d), we have recorded EDX at two different positions: one on the nanodroplet-rich region and the other on the microball. We found that the elemental atomic percentage for both the samples was nearly the same when EDX was recorded at either the nanodroplet-rich region or the microball. However, the atomic percentages of elements were different at different points of measurement, *i.e.*, nanodroplet and microball. The atomic percentages of elements like Si and O were relatively higher for the microballs than that for the nanodroplet-rich region. The atomic percent values of Cd, S, O and Si were estimated to be ~4.2, 3.8, 63.7, and 28.3, respectively, for the nanodroplets; moreover, these values were ~3.0, 2.5, 65.8, and 28.7, respectively, for the microballs more or less irrespective of the annealing temperature. The presence of Au was due to the coating of gold (Au) on the samples for SEM measurements.

3.2 Gas sensing performance of the sensor

3.2.1 Measurement of gas response. A schematic of the device used for gas sensing studies is illustrated in Fig. 4a. The gas response studies of S_0, S_1, S_2, and S_3 were carried out by measuring the disparity in the electrical resistance of the films with varying temperature in the absence/presence of LPG; the results were calculated using eqn (1). Fig. 4b shows the temperature-dependent resistance of the sensors in the absence (R_a)/presence (R_g) of LPG. It is evident from Fig. 4b that the change in the resistance in the presence of LPG at any temperature is opposite for the two types of films: for S_0, the resistance decreases in the presence of LPG, whereas an increase in resistance for S_1, S_2, and S_3 is observed. This signifies that the nature of S_0 is n-type, whereas it is p-type for S_1, S_2, and S_3 as the resistance decreases for the former and increases for the latter in the presence of reducing gas. The insets are the close-ups of surface morphology for the corresponding sensors. The importance of NDs in surface morphology is illustrated here as S_1 with no NDs, which shows an almost negligible change in R_g in the presence of LPG. In contrast, for S_3 with a few droplets/particles, R_g attains a slightly better value. Combining these observations, it is noticed here that a web-like structure filled with CdS NDs over silica MBs is the most suitable structure for LPG sensing. The interrelation of surface morphology and gas sensing studies will be discussed in detail later.

Fig. 5 shows the temperature-dependent LPG responses of different sensors under 1000 ppm gas concentration. The highest response observed was ~71% for S_2 at room temperature (RT); it remained constant up to the operating temperature (OT) of 75 °C and then decreased to ~35% at OT of 100 °C, which is approximately seven times and three times the responses of S_1 and S_3, respectively, over the entire range of OT. Here, it is noticeable that the responses of all the composite films remained nearly stable up to OT of 75 °C. Although the response from S_0 at RT was almost half (~38%) the response of S_2, it was still quite good compared to those of other composite

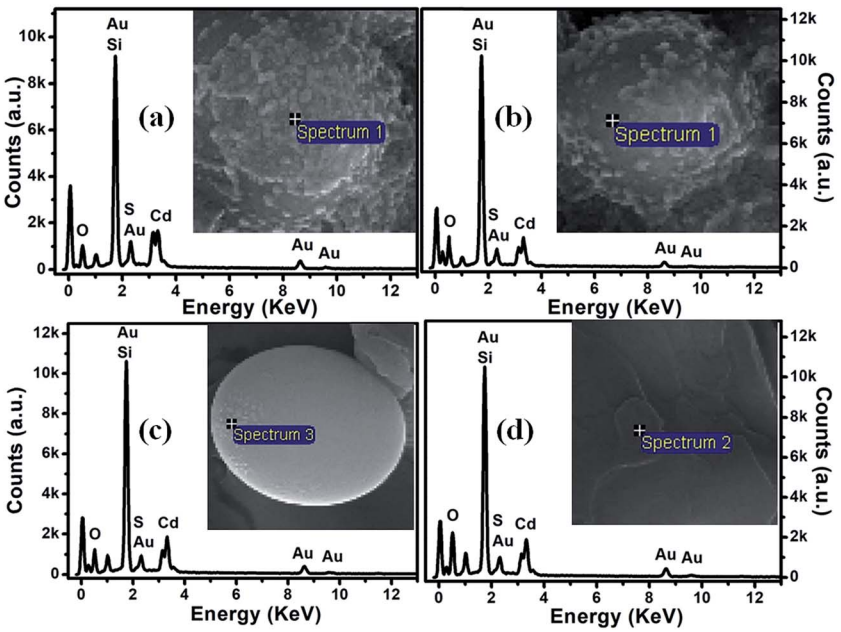

Fig. 3 EDX spectra for CdS:SiO_2 films annealed at 400 °C (a and b) and 500 °C (c and d). Inset: FESEM images with a pointer from where the EDX is taken.

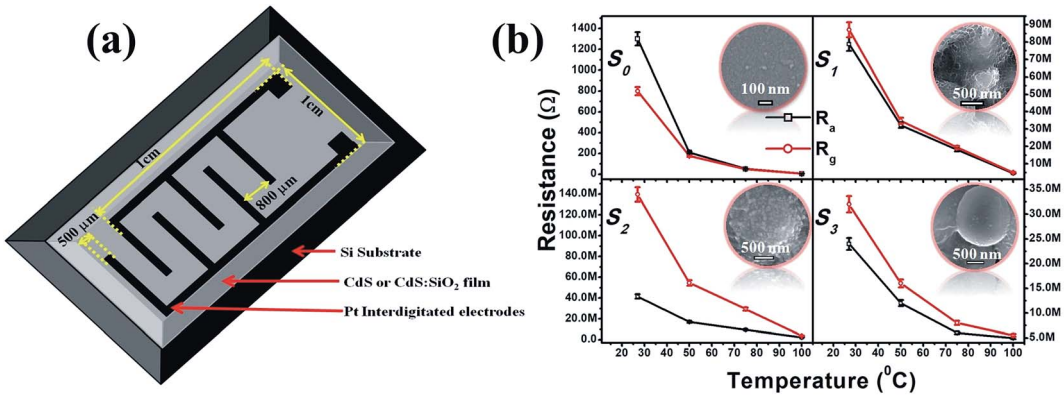

Fig. 4 (a) Schematic of CdS or CdS:SiO_2 thin film-based sensing device structure and (b) temperature-dependent resistance of S_0, S_1, S_2, and S_3 in the absence/presence of LPG. Insets show the corresponding morphologies of the sensors. Black and red lines show the resistances of the sensing device in the absence (R_a) and presence (R_g) of LPG, respectively.

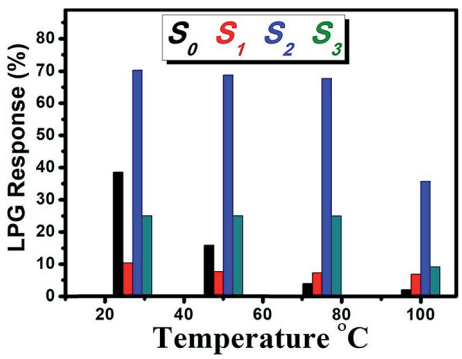

Fig. 5 Variation of responses of different sensors as a function of operating temperature.

films. However, the problem with S_0 is the consistent weakening of response with OT, which limits its performance as a gas sensor above RT. The response from S_0 remained roughly one third at OT of 50 °C and only 2% at OT of 100 °C. In contrast, S_1, S_2, and S_3 could work up to OT of 75 °C with a negligible drop in the response, which indicated the capability of the sustainable gas response of the SiO_2 matrix as far as OT is concerned.

This inquisitive behavior of S_1, S_2, and S_3 towards LPG depends on the microstructures of the films and can be explained as follows: the highest response shown by S_2 is because of high porosity due to the presence of CdS NDs, which offers a high surface area for the reaction with a target gas that correlates with the high response. Furthermore, the web-like structure may lead to significant enhancement in the dangling bonds or improved surface activity for the reaction of the reducing gas with the adsorbed oxygen molecules. In addition, a fast transport of gas molecules is feasible through the porous structures; thereby, the sensor responds faster. The degradation in the response observed for pristine S_1 relative to that observed for S_2 is because of the absence of no clear evolution of CdS nanoparticles (Fig. 2(b) and ESI Fig. S2†) or the generation of the crystalline phase of CdS, as observed by XRD and Raman spectroscopy (please see ESI Fig. S3†). However, S_3 exhibits a lower response due to a lack of the web-like structure along with reduction in the density of CdS droplets/particles on the surface of SiO_2 balls (Fig. 2(d)). Moreover, the diminished response monitored from S_0 compared to that of S_2 is due to the exposure of less surface to the targeting gas, which is due to the smooth/nonporous surface of the film (Fig. 2(a)). Therefore, only S_2 was used to carry out further gas sensing studies.

3.2.2 Selectivity of the sensor. Selectivity is defined as the ability of a sensor to respond to a certain gas under exposure to other gases. However, the selectivity of a sensor in relation to a definite gas is closely connected to its OT. Indeed, selectivity is measured in terms of the selectivity coefficient/factor of a target gas to another gas and given by $K = S_A/S_B$, where S_A and S_B are the responses of a sensor to a target gas "A" and an interference gas "B", respectively.[6]

To estimate the selectivity of S_2 to LPG at optimum OT, *i.e.*, RT, the gas responses towards H_2, H_2S, CO_2, and NO_2 at a concentration of 1000 ppm each were also measured, as shown in the inset of Fig. 6a. The selectivity coefficient for S_2 was the lowest for H_2 (~2.5) and highest for NO_2 (~5.9). A higher K value implies a more selective response to LPG under exposure to other gases. For instance, the gas response to LPG was ~5.9 times higher than that for NO_2. Thus, the experimental results indicate that the sensor presented here has good selectivity for LPG.

3.2.3 Effect of gas concentration. Fig. 6b illustrates the gas response of S_2 at optimum OT, *i.e.*, RT to LPG with concentrations varying from 1 to 1000 ppm. It can be seen that the gas response increases exponentially as a function of LPG concentration. The gas response changes from 0.1 to ~71% in the investigated range. The sensor has a remarkably low detection limit of 20 ppm for LPG with a response of S ~5% at RT. However, a significant response (*i.e.*, 25%) was recorded for 50 ppm concentration of LPG.

3.2.4 Dynamic response of the sensor. The response transients of S_2 under exposure to 1000 ppm LPG at various OTs are shown in Fig. 7(a–d). The curves indicate that under exposure to LPG, the resistance increases sharply at the initial stage and then saturates after a certain time. Similarly, the resistance

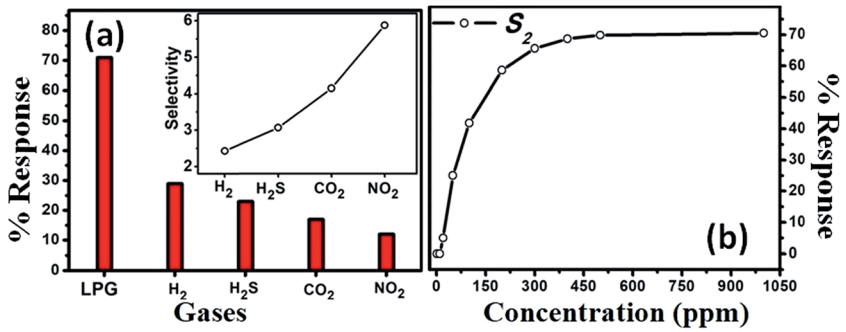

Fig. 6 (a) Response of the LPG sensor S_2 with respect to different gases at a concentration of 1000 ppm. Inset shows the selectivity of sensor S_2 under various gases at RT. (b) LPG gas response as a function of concentration.

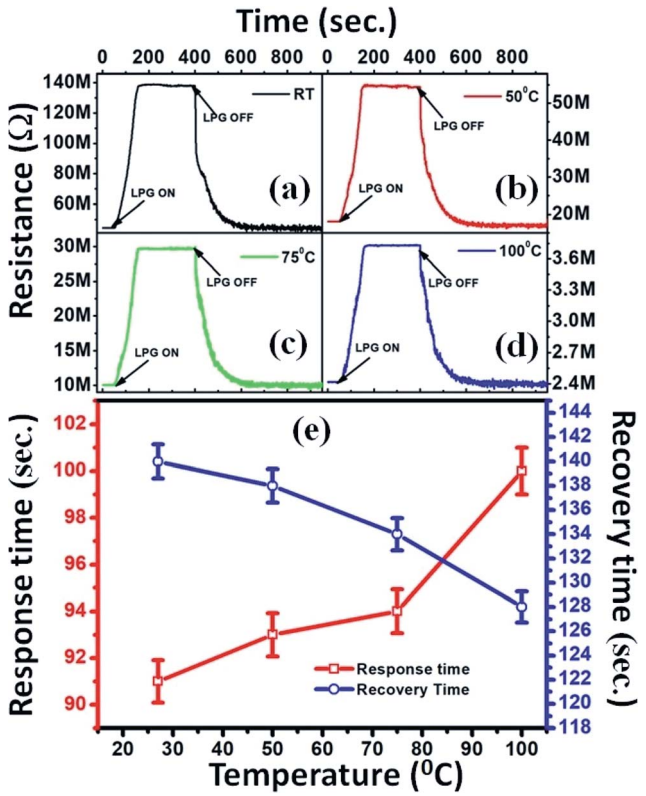

Fig. 7 (a–d) Reproducibility curves at different operating temperatures and (e) variation of response and recovery times with operating temperatures of LPG sensor under 1000 ppm concentration.

drops off rapidly at the initial stage and finally attains nearly its initial value (R_a).

The response and recovery times are crucial parameters for a sensor. The response time (t_r) is measured as the time taken by the sensor to acquire 90% of its maximum resistance value in the presence of the target gas. In contrast, the time taken by the sensor to reacquire about 10% of the higher value of its initial resistance in the absence of gas is considered as the recovery time (t_d).[9] Fig. 7(e) demonstrates the variation in t_r and t_d as a function of OT under exposure to 1000 ppm of LPG. It is observed that t_r and t_d follow opposite trends: the former consistently increases, whereas the latter decreases with an increase in OT. The optimal t_r value observed here is 91 s at RT, whereas t_d is 128 s at OT of 100 °C. However, t_d at RT is slightly larger (~140 s) than optimal t_d. For comparison, we have also recorded the reproducibility curve for S_0 (ESI Fig. S4†); we found that the values of t_r and t_d for S_2 are much better than those (t_r = 256 s and t_d = 466 s) estimated for S_0.

3.2.5 Stability of sensor's response. Long-term stability is another key factor for gas sensors. To examine the stability of the sensor's response with respect to varying humidity conditions, we repeated sensing experiments up to 8 weeks with an interval of one week, as shown in Fig. 8. One can see that the sensor S_2 retains ~96% of its initial response even at OT of 100 °C, indicating the long-lasting performance of sensor S_2. A comparison of the sensing parameters of the room-temperature LPG sensors developed till date is given in Table 1 below.

3.2.6 Mechanism for LPG sensing. The presence of chemisorbed oxygen molecules on the surface of the sensor is the mechanism for LPG sensing, which considerably dominates in nanostructured materials. There is high probability for the absorbance of a certain amount of oxygen from air on the surface of the film. The interaction of semiconducting materials with oxygen occurs by transferring the electrons from the conduction band of the semiconductor to the adsorbed oxygen atoms. The transfer of electrons results in the formation of ionic

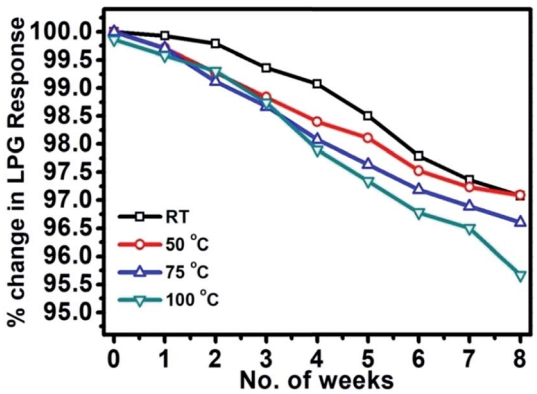

Fig. 8 Percent change in LPG response as a function of time.

Table 1 Demonstrates the comparison of the results obtained here with the outcomes of other studies for room-temperature LPG sensing

Sensing material	Sensitivity/% response	Response/recovery time (s)	LPG conc. (ppm)	Detectivity (ppm)/stability (%)	Ref.
n-CdS/p-polyaniline heterojunction	80	105/165	1040	95% after 30 days	6
CdS/polyacrylamide and $Cd(NO_3)_2 \cdot (AAm)_4 \cdot 2H_2O$ thick films annealed at 450 °C for 2 h	3.7 GΩ min^{-1}	120/480	50 000	97% after 30 days	7
CdS nanowires with PbS nanoparticle surface	60	102/75	1200	93% after 10 days	8
PEDOT:PSS shell on CdS nanowires	58.9	126/109	900	94% after 10 days	9
Cu_2SnS_3/CdS	56	31/56	780	95% after 60 days	10
ZnSnO3/ZnO nanowire					11
n-CdTe/p-polyaniline	67.7	80/200	1400		16
Copper ferrite system ($CuFe_2O_4$)	0.70 MV min^{-1} & 2.6	30/200	10 000		17
Perovskite type neodymium iron oxide film ($NdFeO_3$)	0.47 MΩ s^{-1}	60/90	50 000		18
Nanorods and mixed shaped copper ferrite ($CuFe_2O_4$)	2.6	150/510	10 000		19
p-Polyaniline/*n*-TiO_2 heterojunction	63	140/180	1000		20
p-Polyaniline/*n*-ZnO thin film heterojunction	81	100/150	1040	90% after 30 days	21
SnO_2 thin film sensor loaded with Pt catalyst clusters under UV radiation	44	520/620	200	No significant change after 60 days	22
Nanonail-structured ferric oxide thick film	50	120/150	20 000		23
Polypyrrole (Ppy)/TiO_2 heterojunction	55	112/131	1040		24
Conductive cotton threads functionalized using carbon nanotubes (CNTs) and PANI/g-Fe_2O_3 nanostructures	0.91	25/40	50	50 ppm	25
Cu_2ZnSnS_4 (CZTS)	19.3	70/40	1200	96% after 50 days	26
n-Bi_2S_3-p-CuSCN heterojunction	70	180/142	1370	93% after 14 days	27
p-Polyaniline/*n*-PbS heterojunction	70	125/200	600		28
p-Polyaniline/n-PbS heterojunction	70		780	260 ppm	29
ZnS/polyacrylamide and PbS/polyacrylamide nanocomposites.	62 and 285	180/480 and 120/300	50 000	83% and 91% after 90 days	30
Zinc ferrite nanorods	140	60/300	2000	93% after 60 days	31
CdO necklace-like nanobeads decorated with PbS nanoparticles	51	150/134	1176	94.5% after 8 days	32
ZnO–TiO_2-PANI composite	87	99/118	2000		33
CdS:SiO_2 NCTF annealed at 400 °C (S_2)	71	91/140	1000	20 ppm/97% after 60 days	Present work

species like O_2^- or O^-. The following reactions may be used to elucidate the reaction kinetics:[33,34]

$$O_2\uparrow \leftrightarrow O_{2(ads)} \quad (2)$$

$$O_{2(ads)} + e^- \leftrightarrow {O_{2(ads)}}^- \quad (3)$$

or

$${O_{2(ads)}}^- + e^- \rightarrow 2{O_{(ads)}}^- \quad (4)$$

In this way, the channel conduction is reduced due to the generation of a low-conductive depletion layer near the surface. For sensors that are operable at RT, adsorbed O_2^- ions on the sensor's surface are crucial to improve the receptor capacity of the sensor and thereby its sensing response.[33] The equilibrium of the chemisorption process (state of saturation) is achieved as a result of the stabilization of surface resistance (R_a). The procedure for the stabilization of a sensors' resistance (for S_2) is shown in Fig. 9 through different steps. A schematic of the surface morphology of S_2 is shown in Fig. 9a; Fig. 9b shows magnification of the encircled portion (CdS NDs over SiO_2 MB) with the adsorption of oxygen molecules from the ambient and thermally excited conduction electrons. The electron donation by the sensor to the oxygen and chemisorption of the oxygen molecules/atoms on the surface of the sensor result in a transient state in the resistance, as represented by Fig. 9c. Fig. 9d shows the state when all the conduction electrons are captured by oxygen molecules, *i.e.*, the saturation state of the sensor's resistance. Finally, Fig. 9e shows the stabilization curve of the sensor's resistance with time.

The reducing hydrogen species is bound to the carbon in the constituent molecules such as CH_4, C_3H_8, and C_4H_{10} of LPG; therefore, LPG dissociates into the reactive reducing components on the sensor's surface. Once the sensor is exposed to a reducing gas like LPG, the gas will react with the adsorbed O_2^- or O^-, as shown in eqn (5) and (6) and release the trapped electrons back to the conduction band. This leads to an increased carrier concentration in the n-type semiconductor nc-CdS, which results in decrease in the resistance of the sensor S_0; however, the released electrons from the reaction recombine with the holes in the p-type semiconductors S_1, S_2, and S_3, which increases the resistance.[33,34]

$$C_nH_{2n+2} + O_2^- \rightarrow 2H_2O + C_nH_{2n-2} + e^- \quad (5)$$

or

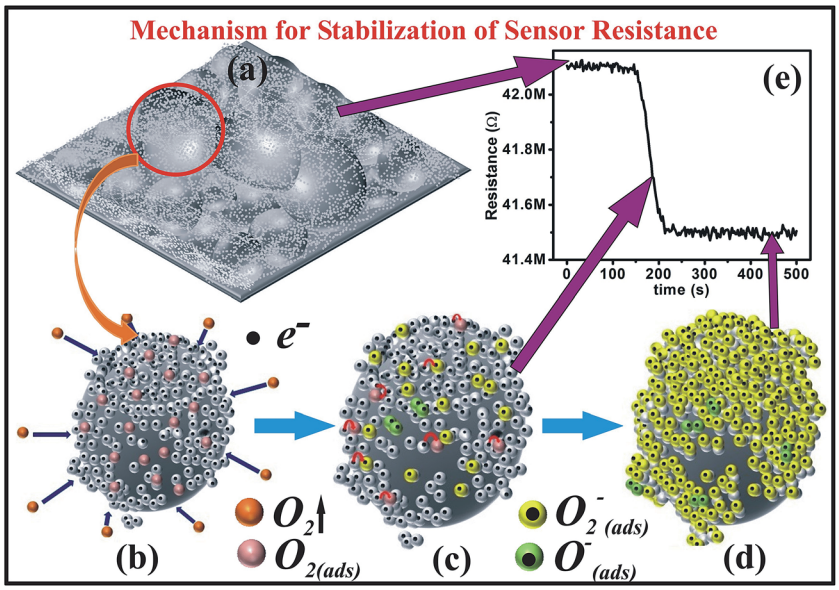

Fig. 9 Schematic representation of the stabilization of sensor resistance.

$$C_nH_{2n+2} + 2O^- \rightarrow H_2O + C_nH_{2n}O^- + e^- \quad (6)$$

Here, C_nH_{2n+2} represents CH_4, C_3H_8, and C_4H_{10}. The reaction continues till all the sensing sites are adsorbed. At this stage, LPG covers all the sensing sites present on the surface of the sensing film, which prevents further reaction of LPG with the chemisorbed oxygen, *i.e.*, saturation is attained; this results in constant resistance. Fig. 10 shows the experimental representation of the response and recovery times of S_2. As LPG is injected into the chamber, it starts to react on the surface of the chemisorbed oxygen, as illustrated by Fig. 10a, which results in a transient state in the sensor's resistance. Fig. 10b demonstrates the maximum possible reaction of the gas molecules with the chemisorbed oxygen, *i.e.*, the saturation state of the sensor's resistance. When LPG is extracted from the chamber and fresh air is injected into the chamber, removal of C_nH_{2n-2} and $C_nH_{2n}O^-$ complexes along with water vapour takes place. This is followed by chemisorption of oxygen on the sensor's surface (Fig. 10c). Fig. 10d corresponds to the gas sensing characteristic of S_2.

Fundamentally, the adsorption/desorption of gas molecules on the surface of a sensor is responsible for the change in the resistance of the film. Here, the highest response was exhibited by sensor S_2 as compared to those of others, which can be

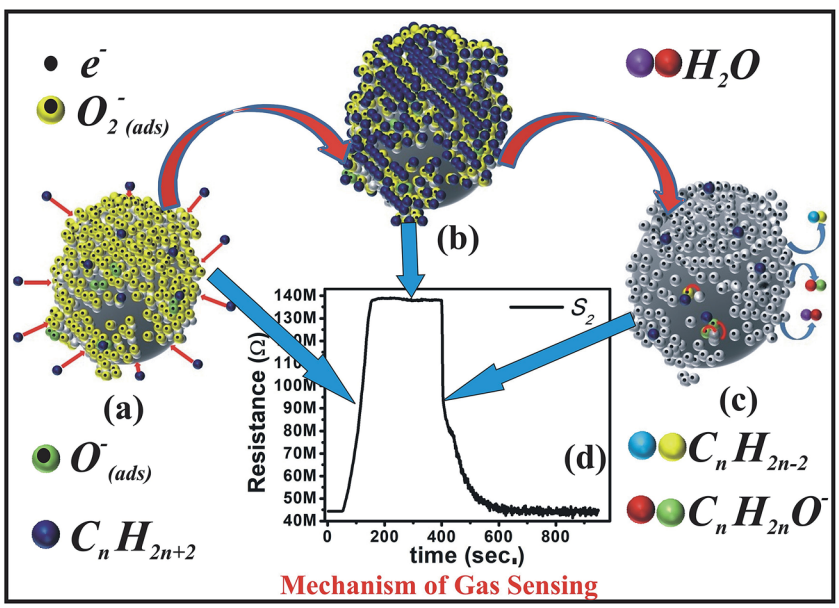

Fig. 10 Schematic illustration of the dynamic study of S_2 with LPG.

explained as follows: the smooth surface and highly packed CdS nanoparticles construct a nonporous surface and the relatively large particle size reduces the surface-to-volume ratio (Fig. S1 and S3†). As a fused effect, S_0 offers less reactive sites for the target gas, which is reflected in terms of the response. The web- or gel-like structure with large porosity in S_1 also cannot offer a large surface area to the target gas for the reaction due to the absence of CdS NDs. In contrast, the reduced density of CdS NDs over the surface of SiO_2 MBs and reduced porosity are jointly responsible for the less reaction sites for the target gas in S_3, which results in a low response. Furthermore, most of the sensors reported in literature are fabricated with the aim of operating either at RT (20 °C) or at a higher temperature. Nevertheless, the sensors that can operate even at lower temperatures than RT are equally important in the perspective of colder regions. The insightful observation of the current study appreciably demonstrates that the sensor presented here may operate at lower OT with either a better or equal response and accomplish the necessity of people residing in relatively colder provinces and save them from LPG leakage-induced fire accidents.

4 Conclusions

The gas sensing characteristics have been inspected for pulsed laser-deposited nc-CdS and CdS:SiO_2 NCTFs. The highest response achieved was ~71% for CdS:SiO_2 NCTF annealed at 400 °C (S_2) at room temperature (27 °C) with relative humidity of ≈60% under exposure to 1000 ppm LPG due to the presence of CdS nanodroplets on micron-sized spherical balls of SiO_2. The sensor presented here demonstrated fast response and recovery times of 91 s and 140 s, respectively. It exhibited high selectivity for LPG and an outstanding detection limit of up to ~20 ppm with a response of 5%. The sensor response was sustained up to OT of 75 °C and it showed enduring stability of ~96% till 8 weeks. The present sensor exhibited either comparable or superior sensing features to those of the sensors reported in literature for LPG detection at room temperature. The performance parameters accomplished here by the sensor are moderately appreciable for practical applications, particularly for the detection of inflammable and hazardous gases such as LPG. The outstanding feature of the present sensor is that it may operate even at lower temperatures than RT (20 °C) with same or higher response, which can save the lives and wealth of the inhabitants of colder areas.

Conflicts of interest

There are no conflicts to declare.

Acknowledgements

The author NS is grateful to the Council for Scientific and Industrial Research (CSIR), New Delhi, India for providing Senior Research Associateship under the Scientists' Pool Scheme (Pool no. 8920-A). One of the author PK is thankful to Science and Engineering Research Board (SERB), New Delhi, India for providing funding under the project ECR/2016/001468 and University Grants Commission, New Delhi, India for providing financial assistance under the UGC Start-Up scheme (30-352/2017(BSR)).

References

1 www.nfpa.org.
2 http://ncrb.gov.in.
3 http://www.academygps.ru.
4 *Nanomaterials Chemistry: Recent Developments and New Directions*, ed. C. N. R. Rao, A Müller, and A. K. Cheetham, Wiley-VCH Verlag GmbH & Co. KGaA, Weinheim, 2007.
5 P. Wang, P. Deng, Y. Nie, Y. Zhao, Y. Zhang, L. Xing and X. Xue, Synthesis of CdS nanorod arrays and their applications in flexible piezo-driven active H_2S sensors, *Nanotechnology*, 2014, **25**, 075501.
6 D. S. Dhawale, D. P. Dubal, V. S. Jamadade, R. R. Salunkhe, S. S. Joshi and C. D. Lokhande, Room temperature LPG sensor based on n-CdS/p-polyaniline heterojunction, *Sens. Actuators, B*, 2010, **145**, 205–210.
7 S. Singh, M. Singh, B. C. Yadav, P. Tandon, S. I. Pomogailo, G. I. Dzhardimalieva and A. D. Pomogailo, Experimental investigations on liquefied petroleum gas sensing of $Cd(NO_3)_2 \cdot (AAm)_4 \cdot 2H_2O$ and CdS/polyacrylamide synthesized via frontal polymerization, *Sens. Actuators, B*, 2011, **160**, 826–834.
8 N. B. Sonawane, K. V. Gurav, R. R. Ahire, J. H. Kim and B. R. Sankapal, CdS nanowires with PbS nanoparticles surface coating as room temperature liquefied petroleum gas sensor, *Sens. Actuators, A*, 2014, **216**, 78–83.
9 N. B. Sonawane, R. R. Ahire, K. V. Gurav, J. H. Kim and B. R. Sankapal, PEDOT:PSS shell on CdS nanowires: room temperature LPG sensor, *J. Alloys Compd.*, 2014, **592**, 1–5.
10 A. C. Lokhande, A. A. Yadav, Ju Y. Lee, M. He, S. J. Patil, V. C. Lokhande, C. D. Lokhande and J. H. Kim, Room temperature liquefied petroleum gas sensing using Cu_2SnS_3/CdS heterojunction, *J. Alloys Compd.*, 2017, **709**, 92–103.
11 Y. Fu, Y. Nie, Y. Zhao, P. Wang, L. Xing, Y. Zhang and X. Xue, Detecting liquefied petroleum gas (LPG) at room temperature using $ZnSnO_3$/ZnO nanowire piezo-nanogenerator as self-powered gas sensor, *ACS Appl. Mater. Interfaces*, 2015, **7**, 10482–10490.
12 P. Kumar, N. Saxena, S. Dewan, F. Singh and V. Gupta, Giant UV-sensitivity of ion beam irradiated nanocrystalline CdS thin films, *RSC Adv.*, 2016, **6**, 3642–3649.
13 N. Saxena, P. Kumar and V. Gupta, Target swapping in PLD: An efficient approach for CdS/SiO_2 and CdS:Ag(1%)/SiO_2 nanocomposite thin films with enhanced luminescent properties, *J. Lumin.*, 2017, **186**, 62–67.
14 P. Kumar, N. Saxena, F. Singh and A. Agarwal, Nanotwinning in CdS quantum dots, *Phys. B*, 2012, **407**, 3347–3351.
15 N. Saxena, P. Kumar and V. Gupta, CdS:SiO_2 nanocomposite as a luminescence-based wide range temperature sensor, *RSC Adv.*, 2015, **5**, 73545–73551.

16 S. S. Joshi, T. P. Gujar, V. R. Shinde and C. D. Lokhande, Fabrication of n-CdTe/p-polyaniline heterojunction-based room temperature LPG sensor, *Sens. Actuators, B*, 2008, **132**, 349–355.
17 S. Singh, B. C. Yadav, V. D. Gupta and P. K. Dwivedi, Investigation on effects of surface morphologies on response of LPG sensor based on nanostructured copper ferrite system, *Mater. Res. Bull.*, 2012, **47**, 3538–3547.
18 S. Singh, A. Singh, B. C. Yadav and P. K. Dwivedi, Fabrication of nanobeads structured perovskite type neodymium iron oxide film: its structural, optical, electrical and LPG sensing investigations, *Sens. Actuators, B*, 2013, **177**, 730–739.
19 S. Singh, B. C. Yadav, R. Prakash, B. Bajaj and J. Rock lee, Synthesis of nanorods and mixed shaped copper ferrite and their applications as liquefied petroleum gas sensor, *Appl. Surf. Sci.*, 2011, **257**, 10763–10770.
20 D. S. Dhawale, R. R. Salunkhe, U. M. Patil, K. V. Gurav, A. M. More and C. D. Lokhande, Room temperature liquefied petroleum gas (LPG) sensor based on p-polyaniline/n-TiO_2 heterojunction, *Sens. Actuators, B*, 2008, **134**, 988–992.
21 D. S. Dhawale, D. P. Dubal, A. M. More, T. P. Gujar and C. D. Lokhande, Room temperature liquefied petroleum gas (LPG) sensor, *Sens. Actuators, B*, 2010, **147**, 488–494.
22 D. Haridas, A. Chowdhuri, K. Sreenivas and V. Gupta, Enhanced room temperature response of SnO_2 thin film sensor loaded with Pt catalyst clusters under UV radiation for LPG, *Sens. Actuators, B*, 2011, **153**, 152–157.
23 B. C. Yadav, S. Singh and A. Yadav, Nanonails structured ferric oxide thick film as room temperature liquefied petroleum gas (LPG) sensor, *Appl. Surf. Sci.*, 2011, **257**, 1960–1966.
24 R. N. Bulakhe, S. V. Patil, P. R. Deshmukh, N. M. Shinde and C. D. Lokhande, Fabrication and performance of polypyrrole (Ppy)/TiO_2 heterojunction for room temperature operated LPG sensor, *Sens. Actuators, B*, 2013, **181**, 417–423.
25 N. G. Shimpi, D. P. Hansora, R. Yadav and S. Mishra, Performance of hybrid nanostructured conductive cotton threads as LPG sensor at ambient temperature: preparation and analysis, *RSC Adv.*, 2015, **5**, 99253–99269.
26 K. V. Gurav, S. W. Shin, U. M. Patil, P. R. Deshmukh, M. P. Suryawanshi, G. L. Agawane, S. M. Pawar, P. S. Patil, J. Y. Lee, C. D. Lokhande and J. H. Kim, Cu_2ZnSnS_4 (CZTS)-based room temperature liquefied petroleum gas (LPG) sensor, *Sens. Actuators, B*, 2014, **190**, 408–413.
27 R. D. Ladhe, P. K. Baviskar, W. W. Tan, J. B. Zhang, C. D. Lokhande and B. R. Sankapal, LPG sensor based on complete inorganic n-Bi_2S_3-p-CuSCN heterojunction synthesized by a simple chemical route, *J. Phys. D: Appl. Phys.*, 2010, **43**, 245302.
28 S. V. Patil, P. R. Deshmukh and C. D. Lokhande, Fabrication and liquefied petroleum gas (LPG) sensing performance of p-polyaniline/n-PbS heterojunction at room temperature, *Sens. Actuators, B*, 2011, **156**, 450–455.
29 R. N. Bulakhe and C. D. Lokhande, Chemically deposited cubic structured CdO thin films: use in liquefied petroleum gas sensor, *Sens. Actuators, B*, 2014, **200**, 245–250.
30 S. Singh, A. Singh, B. C. Yadav, P. Tandon, S. Kumar, R. R. Yadav, S. I. Pomogailo, G. I. Dzhardimalieva and A. D. Pomogailo, Frontal polymerization of acrylamide complex with nanostructured ZnS and PbS: their characterizations and sensing applications, *Sens. Actuators, B*, 2015, **207**, 460–469.
31 A. Singh, A. Singh, S. Singh, P. Tandon, B. C. Yadav and R. R. Yadav, Synthesis, characterization and performance of zinc ferrite nanorods for room temperature sensing applications, *J. Alloys Compd.*, 2015, **618**, 475–483.
32 N. B. Sonawane, P. K. Baviskar, R. R. Ahire and B. R. Sankapal, CdO necklace like nanobeads decorated with PbS nanoparticles room temperature LPG sensor, *Mater. Chem. Phys.*, 2017, **191**, 168–172.
33 R. K. Sonker, B. C. Yadav, V. Gupta and M. Tomar, Fabrication and characterization of ZnO-TiO_2-PANI (ZTP) micro/nanoballs for the detection of flammable and toxic gases, *J. Hazard. Mater.*, 2019, **370**, 126–137.
34 K. R. Nemade and S. A. Waghuley, LPG sensing application of graphene/Bi_2O_3 quantum dots composites, *Solid State Sci.*, 2013, **22**, 27–32.